Impact of product gas recycling on steam methane reforming performance with Ni and Rh catalysts

Ali Saeedi* | Fatemeh Zangooei

Department of Mechanical Engineering, Faculty of Engineering, University of Birjand, Iran

* Corresponding author, Email: ali.saeedi@birjand.ac.ir

Article Information

Abstract

This study investigates the impact of gas product recycling (GPR) on the performance of the steam methane reforming (SMR) process using nickel (Ni) and rhodium (Rh) catalysts. Hydrogen production, a cleaner alternative to fossil fuels, predominantly employs SMR due to its industrial efficacy. The study utilizes numerical simulations with Cantera software to evaluate the effects of recycling up to 30% of gaseous products at temperatures of 800, 1000, and 1200 Kelvin and a steam-to-methane ratio of 3. Key governing equations, including mass and energy conservation, as well as reaction kinetics described by the Arrhenius equation, are applied. The simulations reveal that GPR at 1200 K with a Ni catalyst enhances syngas production and reduces CO_2 leakage, making it a viable option within the 20-30% recycling range. However, GPR at lower temperatures (800 K and 1000 K) for both Ni and Rh catalysts, and at 1200 K for Rh catalysts, results in undesirable increases in carbon deposition and CO_2 production. Thus, GPR is generally not recommended for Rh catalysts due to significant coke formation. These findings underscore the potential benefits and limitations of GPR in optimizing SMR processes, particularly highlighting the suitability of Ni catalysts at higher temperatures.

1 Introduction

Hydrogen is a clean energy source proposed as an alternative to fossil fuels [1]. Unlike conventional fuels, hydrogen is not readily available in nature, and must be produced from primary energy sources before being used in internal combustion engines and fuel cells. Currently, hydrogen production sources include 48% from natural gas, 30% from heavy oils and naphtha, and 18% from coal. Hydrogen can be produced using various methods such as steam reforming (SR), partial oxidation (POX), autothermal reforming (ATR), pyrolysis, biomass biological processes, and water electrolysis [2]. Among these methods, steam methane reforming (SMR) is particularly developed and cost-effective for producing hydrogen on an industrial scale [3]. Commercial hydrogen is produced through the SMR process with an efficiency of 65-75% at best. The SMR process involves a set of reactions: methane reforming (reactions (1) and (2)), and water-gas shift (WGS) (reaction (3)):

$$CH_4 + H_2O \rightleftharpoons CO + 3H_2, \quad \Delta H_{298} = 206.1 \frac{kJ}{mol} \quad (1)$$

$$CH_4 + 2H_2O \rightleftharpoons CO_2 + 4H_2, \quad \Delta H_{298} = 165.0 \frac{kJ}{mol} \quad (2)$$

$$CO + H_2O \rightleftharpoons CO_2 + H_2, \quad \Delta H_{298} = -41.15 \frac{kJ}{mol} \quad (3)$$
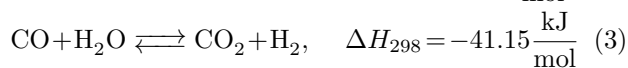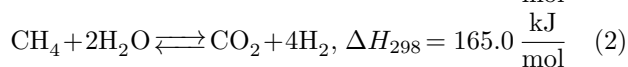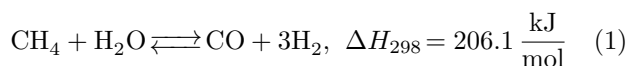
Reactions (1) and (2) are highly endothermic and occur at high temperatures, while reaction (3) is exothermic [4]. Stoichiometrically, reactions (1) and (2) tend to occur at low pressures due to the doubling of gas volume, while pressure changes do not significantly affect reaction (3) [5]. Rhodium and nickel are among the catalysts used in the SMR process. Rhodium is a precious metal with excellent performance, but its scarcity and high cost hinder widespread use [1]. Nickel is an inexpensive transition metal with alloys that exhibit comparable activity to precious metals [6].

Steam methane reforming (SMR) for hydrogen production has been extensively studied from various perspectives. Numaguchi and Kikuchi modeled SMR using a fixed-bed reactor over a nickel catalyst, showing higher intrinsic WGS reaction rates at lower temperatures. Their design simulation in a complex reaction network provided valuable data for optimizing industrial SMR processes [7]. Jianguo and Froment investigated SMR and water-gas shift (WGS) reactions over a $Ni/MgAl_2O_4$ catalyst. They determined intrinsic reaction rates and reduced possible reactions through thermodynamic analysis, providing a comprehensive kinetic model for SMR [8]. Wang and Gorte examined SMR over a Pd/Ceria catalyst and found higher

activity compared to Pd/Alumina. Their study highlighted the superior catalytic performance of Pd/Ceria, which could lead to more efficient hydrogen production processes [9].

Rakass et al. investigated SMR with unpromoted nickel powder catalysts, achieving high methane conversion and catalytic activity at 700 °C without coke formation. Their findings demonstrated the feasibility of using unsupported nickel catalysts for efficient methane reforming [10]. Zhu et al. explored SMR over platinum and rhodium catalysts, demonstrating higher activity for rhodium nanoparticle catalysts. Their microkinetic analysis provided insights into the reaction mechanisms on metal surfaces, emphasizing the potential of rhodium for enhanced hydrogen production [11]. Panagakos et al. highlighted the impact of operational factors on hydrogen production in SMR reactors. Their computational investigation provided insights into optimizing reactor conditions for maximum hydrogen yield [12].

Arora and Prasad addressed catalyst deactivation due to coke formation in methane dry reforming, suggesting hydrogen addition as a preventative measure. Their review offered strategies to mitigate carbonaceous deactivation, contributing to the longevity and efficiency of reforming catalysts [13]. German and Sheintuch proposed a microkinetic model for SMR over Pt (111), Rh (111), and Ni (111) catalysts, noting significant effects of water vapor at low partial pressures. Their model accounted for hydrogen tunneling and metal lattice vibrations, contributing to a better understanding of catalyst performance under various conditions [14]. Abbas et al. studied kinetic data of SMR over a nickel catalyst, demonstrating superior performance at high temperatures, low pressures, and high steam-to-carbon ratios. Their research provided a detailed kinetic model that could be used for reactor design and optimization [15].

Castillo et al. examined SMR under low-temperature conditions with a Ru/Al_2O_3 catalyst, finding high activity and reaction promotion at low pressures. Their microkinetic analysis of the methane steam reforming process contributed to the development of low-temperature catalytic systems [16]. Saeedi and Alahdadi explored methane partial oxidation using a Rh/Al_2O_3 catalyst, improving hydrogen production and CO_2 reduction with gas recirculation. Their numerical investigation demonstrated the benefits of gas product recycling in enhancing catalyst performance [17]. Saeedi and Zangooee compared Ni- and Rh-based catalysts for SMR, revealing higher activity but greater surface coverage for Rh catalysts. Their study provided a comprehensive evaluation of the two catalysts, highlighting the advantages and limitations of each [18].

Previous studies have examined the performance of the SMR process under various conditions, focusing on catalysts and operating parameters. However, the effect of recycling gaseous products to the reactor inlet has not been extensively evaluated. Recycling gaseous products is proposed to enhance SMR yield by triggering reactions that increase hydrogen production. This study uses numerical simulation to model the recycling of SMR process gaseous products to the reactor inlet over nickel and rhodium catalysts. The simulation, conducted using Python and Cantera software, explores recycle fractions up to 30% by volume at atmospheric pressure and temperatures of 800, 1000, and 1200 K, with a steam-to-carbon ratio of 3. The objective is to determine the highly functioning temperature range, recycle volume fraction, and catalyst for recycling SMR process gaseous products to the reactor inlet.

2 Fundamentals and solution method

Numerical solutions were performed using Cantera software in a Python environment. Cantera, developed by Professor David G. Goodwin at the California Institute of Technology, is an open-source software for investigating chemical kinetics, thermodynamic processes, and transport phenomena. Cantera codes are accessible in four programming languages: C++, Python, MATLAB, and Fortran [19]. In this study, the Python environment was chosen for modeling due to its versatility and simplicity.

A plug-flow reactor, depicted schematically in Figure 1, was employed for modeling. This reactor maintains a constant cross-sectional area with its bed coated in catalyst, allowing heterogeneous chemical reactions to occur on the channel walls. The reactor dimensions are on the centimeter scale, while the catalyst bed features a nanometer-scale structure and porosity. As a result, temperature and pressure grad across the reactor can be neglected. In this one-dimensional model, properties only change along the z-axis. In the axial direction, the diffusion term is much smaller than the axial convection term, and in the radial direction, properties are assumed to be uniform, with no dependent variable on this dimension in the equation. Consequently, all diffusion terms are eliminated in the plug-flow equations [16].

The SMR process is simulated by discretizing the plug flow reactor into a series of well-stirred reactors (WSRs). Initial parameters such as temperature, pressure, flow rate, and catalyst properties are set, and governing equations, including mass and energy conservation and reaction kinetics, are applied. The simulation results are validated by comparing them with experimental data to ensure accuracy and reliability.
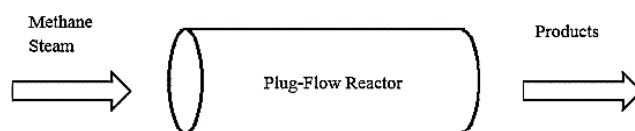

Fig. 1. Schematic of a plug-flow reactor with a cylindrical cross-section.

A plug-flow reactor can be discretized into a finite number of axially distributed volumes. These volumes can be modeled as a chain of continuously stirred tank reactors (CSTRs) in a steady state condition. This modeling approach converts the system of ordinary differential equations into a system of algebraic equations with surface reactions. An upstream source is considered, and its initial conditions are the same as the boundary conditions of the plug-flow reactor. Time integration is performed over the CSTR until convergence is reached, and the steady state of the CSTR is solved. The output state of this reactor becomes the input boundary condition for the next CSTR.

3 Assumptions and modeling

Assumptions in the mathematical model:
- The process is isothermal (constant temperature).
- The process is isobaric (constant pressure).
- The ideal gas law is valid.
- Concentration and temperature gradients in the radial direction are negligible; therefore, only axial concentration changes are considered.
- The bed porosity is uniform.
- Ideal flow (without friction) is assumed.
- The effects of body forces on the fluid are neglected.
- The flow is in a steady state.

Since a co-isothermal plug flow reactor with a catalytic wall is considered, solving the energy equation is not required. Additionally, based on the assumptions, the momentum equation is neglected.

3.1 Continuity equation

The continuity equation for the plug-flow reactor is given by Equation (4) [19].

$$\frac{d(\rho u A)}{dz} = P' \sum_k \dot{s}_k W_k \qquad (4)$$

In the above equation, P' is defined as the active area of the channel per unit length in meters, which can

differ from the channel perimeter P; $\dot{s}_k$ is the chemical source term resulting from the heterogeneous chemical reaction chain.

3.2 Conservation equation of species k

The conservation equation for species k in plug flow reactors is derived using the mass continuity principle, considering both source terms for homogeneous chemistry (where all species are in the gas phase) and heterogeneous chemistry (where reactant species may be in gas or solid phases) [19]:

$$\rho u A \frac{dY_k}{dz} + Y_k P' \sum_k \dot{s}_k W_k = A \dot{\omega}_k W_k + P' \dot{s}_k W_k . \quad (5)$$

3.3 Chemical modeling

A significant portion of chemical processes occur at the interface between a solid surface and the adjacent gases. In this study, homogeneous gas-phase reactions are negligible under the prevailing temperature and pressure conditions, so only heterogeneous reactions are considered.

Each surface can occupy one or more pores on the plate, characterized by surface porosity density. The dynamics of local changes in the surface coverage of adsorbed species are described by Equation (6) [20]:

$$\frac{d\theta_k}{dt} = \frac{\dot{s}_k \sigma_k}{\Gamma} . \quad (6)$$

Under steady-state conditions, Equation (6) is converted into a system of nonlinear algebraic equations [21].

The Arrhenius equation shows that the reaction rate constant is temperature-dependent and can be calculated according to Equation (7):

$$k_{f,i} = A_i T^{\beta_i} \exp\left(-\frac{E_i}{RT} \right) . \quad (7)$$

In most cases, the forward reaction rate constant is calculated according to Equation (7). However, in some cases, the Arrhenius function is modified by certain surface species. Equation (8) incorporates pre-exponential factors and activation energies of the surface species as functions of their surface coverage:

$$k_{f,i} = A_i T^{\beta_i} \exp\left(-\frac{E_i}{RT} \right)$$
$$\times \prod_{k_s} 10^{a_{ki}\theta_{ki}} \theta_{ki}^{m_{ki}} \exp\left(-\frac{\epsilon_{ki}\theta_{ki}}{RT} \right) \quad (8)$$

In heterogeneous reactions, the collision of gas-phase molecules with the solid surface is essential. The adsorption coefficient represents the rate of surface reactions or the rate of potential collisions with the surface leading to a reaction. The adsorption coefficient is highly temperature-dependent and can be calculated according to Equation (9):

$$\gamma_i = a_i T^{b_i} \exp\left(-\frac{c_i}{RT} \right) . \quad (9)$$

The adsorption coefficient is related to the reaction constant through the experimental law of mass action kinetics, as described by Equation (10):

$$k_{f,i} = \frac{\gamma_i}{\Gamma^m} \sqrt{\frac{RT}{2\pi W}} . \quad (10)$$

4 Results and discussion

Thermodynamic simulation is best achieved through an isobaric and isothermal environment [22]. In this study, a one-dimensional reactor mesh is created by stacking zero-dimensional discretized spaces. The output state of each well-stirred zero-dimensional reactor serves as the input boundary condition for the next reactor. This method allows a one-dimensional solution to be obtained from a collection of zero-dimensional solutions. Primary gas-phase reactions were not considered, as they are insignificant under the given conditions.

One proposed method for increasing the performance of the steam methane reforming (SMR) process is to recycle the gaseous products of this process [17]. As shown in Figure 2, a portion of the outlet stream is recycled back to the reactor inlet. The recycled gaseous products include methane, water vapor, hydrogen, carbon monoxide, and carbon dioxide. The gaseous products are recycled up to 30% by volume at atmospheric pressure and temperatures of 800, 1000, and 1200 K, ensuring that the steam-to-carbon ratio (S/C), obtained from Equation (10), remains constant at 3.

$$\text{S/C} = \frac{n_{H_2O,in}}{n_{CH_4,in}} . \quad (11)$$

In this study, the effect of catalyst type, temperature, and volume percentage of recycled gas on the SMR process will be evaluated.
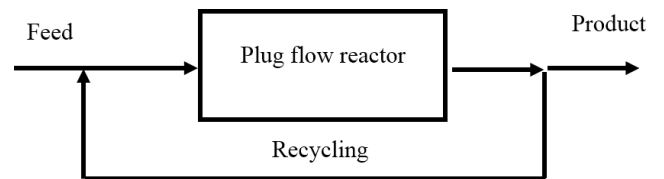

Fig. 2. Schematic diagram of the process for recycling gaseous products to the reactor inlet.

Modeling was performed for each catalyst using a validated chain mechanism, and the numerical results were compared with experimental values for both models. A kinetic model was employed for simulating the steam methane reforming process in the presence of a nickel catalyst with 42 reactions, and a mechanism with 48 reactions was used for the rhodium catalyst [23,24]. The reaction mechanisms for nickel and rhodium catalysts were written in a suitable format in the Cantera software. This study investigates the impact of recycling gaseous products to the reactor inlet on the performance of the steam methane reforming process in the presence of nickel and rhodium catalysts, under the conditions listed in Table 1.

Table 1. Conditions used in modeling for evaluating the performance of nickel and rhodium catalysts.

| Quantity	Value
Catalyst bed length (cm)	2
Reactor hydraulic diameter(mm)	1.6
Nickel catalyst surface porosity density for simulation 1(mol/cm^2)	2.66×10^{-9}
Rhodium catalyst surface porosity density for simulation 2 (mol/cm^2)	2.72×10^{-9}
Catalyst bed porosity	0.3

4.1 Validation of steam methane reforming process in the presence of nickel catalyst

Figure 3 illustrates the comparison between the steam methane reforming process in the presence of a nickel catalyst, as predicted by two kinetic models, and the experimental results obtained by Ryu et al. [25]. The reference values were obtained experimentally using a quartz tube reactor coated with a nickel catalyst, operating at a flow rate of 9000 1/h and maintaining a steam-to-carbon ratio of 3 under atmospheric pressure. The model yields acceptable results, demonstrating a maximum difference of 21.9% between the experimental values and Model 1. This highlights the accuracy of modeling the steam methane reforming process in the presence of a nickel catalyst by employing a set of zero-dimensional reactors to simulate the one-dimensional process using Cantera software.
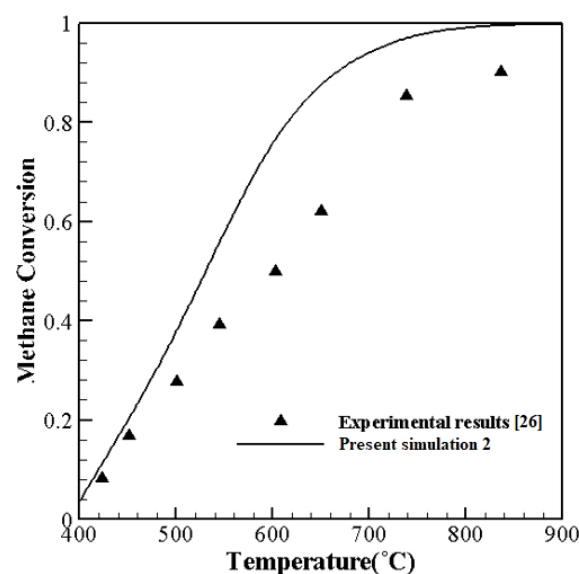
4.2 Validation of steam methane reforming process in the presence of rhodium catalyst

Figure 4 compares the steam methane reforming process in the presence of a rhodium catalyst for the ki-

netic model with the experimental results of Schädel et al. [26]. The reference values were obtained experimentally, completely different from the nickel catalyst, in a quartz tube reactor coated with rhodium catalyst at a flow rate of 40000 1/h and 75% volume Argon to dilute the inlet mixture to the reactor under atmospheric pressure. The kinetic model yields acceptable results, with Model 2 showing a maximum difference of 25.5% from the experimental values, suggesting it is a suitable option for simulating the steam methane reforming process in the presence of a rhodium catalyst.
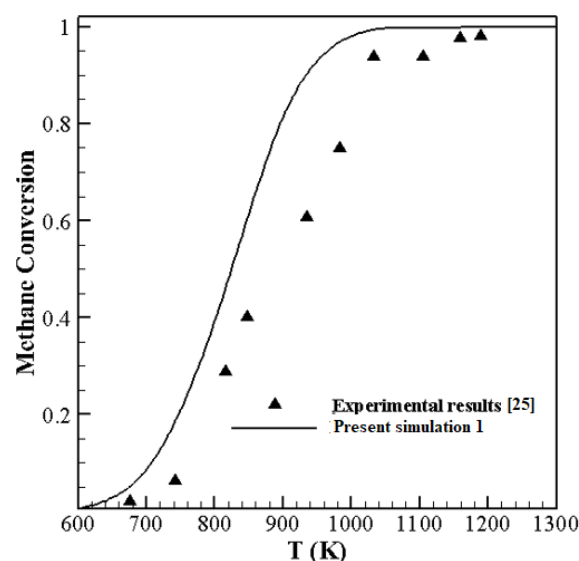
Fig. 3. Validation results of steam methane reforming process in the presence of nickel catalyst for simulation 1 according to mechanism [25].

Fig. 4. Validation results of steam methane reforming process in the presence of rhodium catalyst for simulation 2 according to mechanism [26].

4.3 Evaluation of the effect of gas product recycling on the steam methane reforming process in the presence of nickel catalyst

Figure 5 shows the percentage increase in hydrogen, carbon monoxide, carbon dioxide, and carbon surface coverage at a) 800, b) 1000, and c) 1200 K in the presence of nickel catalyst. As can be observed, temperature has a significant impact on gas product recycling.

At 800 K (Figure 5a) As the volume percentage of recycled gas products increases, the production of H_2, CO, and CO_2 increases, while carbon surface coverage decreases. For example, at 20% recycling volume, the changes in H_2, CO, CO_2, and C(s) species are 2.35%, 4.44%, 2.32%, and −0.29%, respectively. The increase in hydrogen and carbon monoxide production suggests that the recycling of gas products stimulates further reforming reactions, enhancing overall hydrogen yield. However, the concurrent increase in CO_2 production indicates that the water-gas shift reaction is also being promoted, which is less desirable at this temperature. The decrease in carbon surface coverage implies a reduced risk of catalyst deactivation by carbon deposition, which is advantageous for the process.

At 1000 K (Figure 5b) With increasing gas product recycling, the production of H_2, CO, CO_2, and C(s) species increases. For example, at 20% recycling volume, the changes in these species are 3.05%, 7.37%, 1.44%, and 3.3%, respectively. The trends at this temperature reflect a more pronounced enhancement in hydrogen and carbon monoxide production compared to 800 K, which is beneficial for syngas production. The smaller increase in CO_2 production indicates a lesser extent of the water-gas shift reaction, which aligns with the objective of maximizing hydrogen yield. However, the significant increase in carbon surface coverage poses a higher risk of catalyst deactivation due to coke formation, highlighting a critical trade-off at this temperature.

At 1200 K (Figure 5c) Increasing recycling up to 30% volume at 1200 K increases the production of hydrogen, carbon monoxide, and carbon surface coverage while decreasing carbon dioxide. For example, at 20% recycling volume, the changes in H_2, CO, CO_2, and C(s) species are 4.24%, 9.42%, −3.32%, and 9.39%, respectively. The high temperature significantly enhances the reforming reactions, leading to substantial increases in hydrogen and carbon monoxide production. The reduction in CO_2 production indicates a suppression of the water-gas shift reaction, which is desirable for maximizing hydrogen output. However, the considerable increase in carbon surface coverage suggests a heightened risk of coke formation, which could negatively impact the long-term stability of the catalyst. Based on the graphs, it can be inferred that adding a small amount of hydrogen, carbon monoxide, and carbon dioxide through gas product recycling stimulates the chain of chemical reactions, consequently affecting the production of hydrogen, carbon monoxide, and carbon dioxide.

At 800 K The production of additional carbon dioxide is undesirable.

At 1000 K Recycling leads to a simultaneous increase in carbon dioxide production and carbon surface coverage, making recycling less favorable.

At 1200 K Recycling within the range of 20-30% volume is acceptable due to the increased production of syngas and the reduced leakage of additional carbon dioxide.

Therefore, recycling is not recommended at 800 K and 1000 K, but it is acceptable at 1200 K within the specified volume range. The detailed analysis of these trends provides deeper insights into the complex interplay between reaction kinetics and catalyst stability, ensuring a comprehensive understanding of the SMR process under various conditions.

4.4 Evaluation of the effect of gas product recycling on the steam methane reforming process in the presence of rhodium catalyst

Figure 6 shows the percentage increase in hydrogen, carbon monoxide, carbon dioxide, and carbon surface coverage at (a) 800 K, (b) 1000 K, and (c) 1200 K in the presence of a rhodium catalyst. Based on Figure 6, the following results can be achieved:

At 800 K (Figure 6a) Gas product recycling leads to an increase in the production of hydrogen, carbon monoxide, carbon dioxide, and carbon surface coverage. For example, at 30% recycling, the production rates of H_2, CO, CO_2, and C(s) increase by 1.91%, 6.44%, 1.24%, and 4.84%, respectively. The increase in hydrogen and carbon monoxide production indicates that recycling stimulates the reforming reactions, enhancing overall syngas yield. However, the simultaneous rise in CO_2 and carbon surface coverage suggests that the water-gas shift reaction is also active, and there is a risk of increased coke deposition on the catalyst surface, which could impair catalyst performance and longevity.
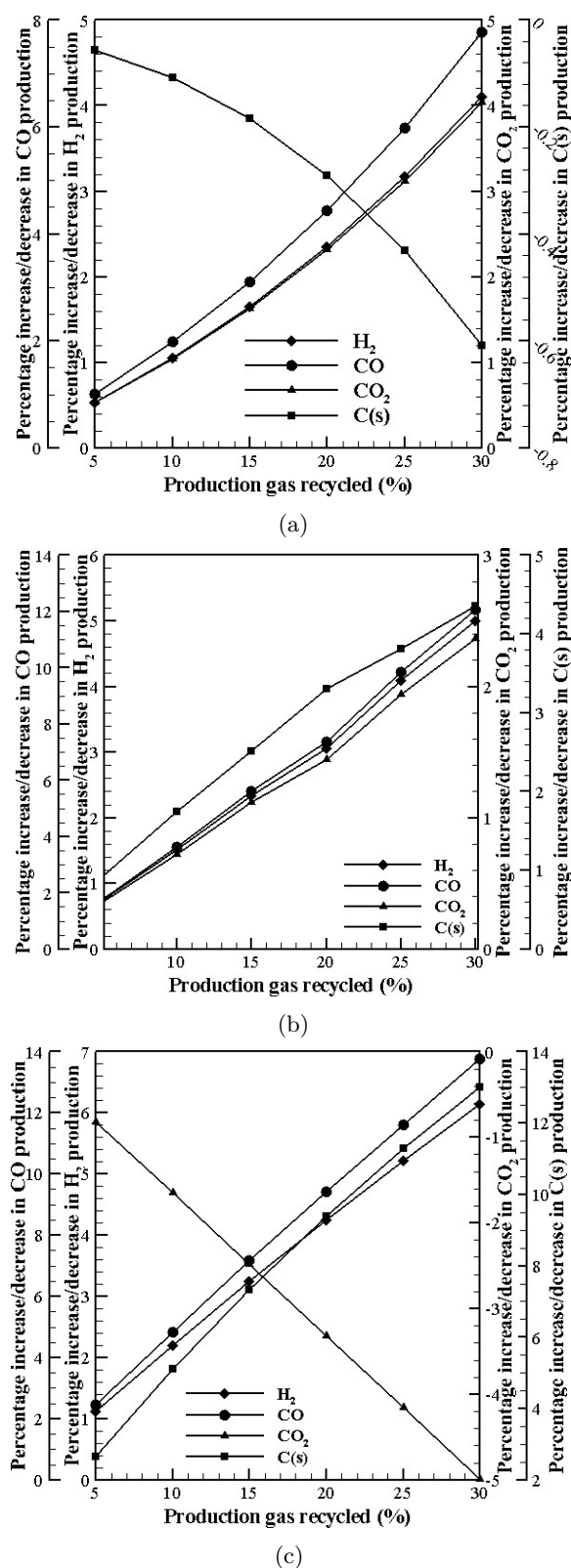
(a)

(b)

(c)

Fig. 5. Evaluation of the effect of gas product recycling on the increase in hydrogen, carbon monoxide, carbon dioxide, and carbon surface coverage at (a) 800 K, (b) 1000 K, and (c) 1200 K, S/C ratio equal to 3, and atmospheric pressure in the presence of nickel catalyst.

At 1000 K (Figure 6b) Increasing recycling up to 30% volume increases the production of hydrogen, carbon monoxide, and carbon surface coverage while decreasing carbon dioxide production. For example, at 30% volume recycling, the production rates of hydrogen, carbon monoxide, and carbon surface coverage increase by 4.57%, 14.21%, and 17.0%, respectively, while carbon dioxide decreases by 5.75%. The trends at this temperature highlight a more favorable scenario for hydrogen and carbon monoxide production, with a reduction in CO_2 suggesting less water-gas shift activity. However, the significant increase in carbon surface coverage indicates a higher risk of coke formation, which could hinder the catalyst's effectiveness and require frequent regeneration or replacement.

At 1200 K (Figure 6c) Increasing recycling up to 30% volume at 1200 K increases the production of hydrogen, carbon monoxide, and carbon surface coverage while decreasing carbon dioxide. For example, at 30% recycling volume, the changes in H_2, CO, CO_2, and C(s) species are 5.73%, 13.26%, −8.95%, and 31.2%, respectively. At this high temperature, the SMR process benefits from enhanced hydrogen and carbon monoxide production, with a notable decrease in CO_2 indicating minimal water-gas shift reaction. Nonetheless, the substantial rise in carbon surface coverage suggests a severe risk of coke formation, potentially leading to rapid catalyst deactivation and increased operational challenges.

Based on the graphs, it can be inferred that adding a small amount of hydrogen, carbon monoxide, and carbon dioxide through gas product recycling stimulates the chain of chemical reactions, consequently affecting the production of hydrogen, carbon monoxide, and carbon dioxide.

At 800 K The increase in carbon dioxide and carbon surface coverage makes recycling at this temperature unsuitable.

At 1000 K Recycling leads to a simultaneous increase in carbon dioxide production and carbon surface coverage, making recycling less favorable.

At 1200 K Recycling within the range of 20-30% volume is not recommended due to the significant increase in coke deposition on the catalyst bed despite the increased production of syngas.

Therefore, gas product recycling is not recommended at 800 K and 1000 K, and it is also not suitable at 1200 K within the specified volume range due to the significant increase in coke deposition on the catalyst bed.
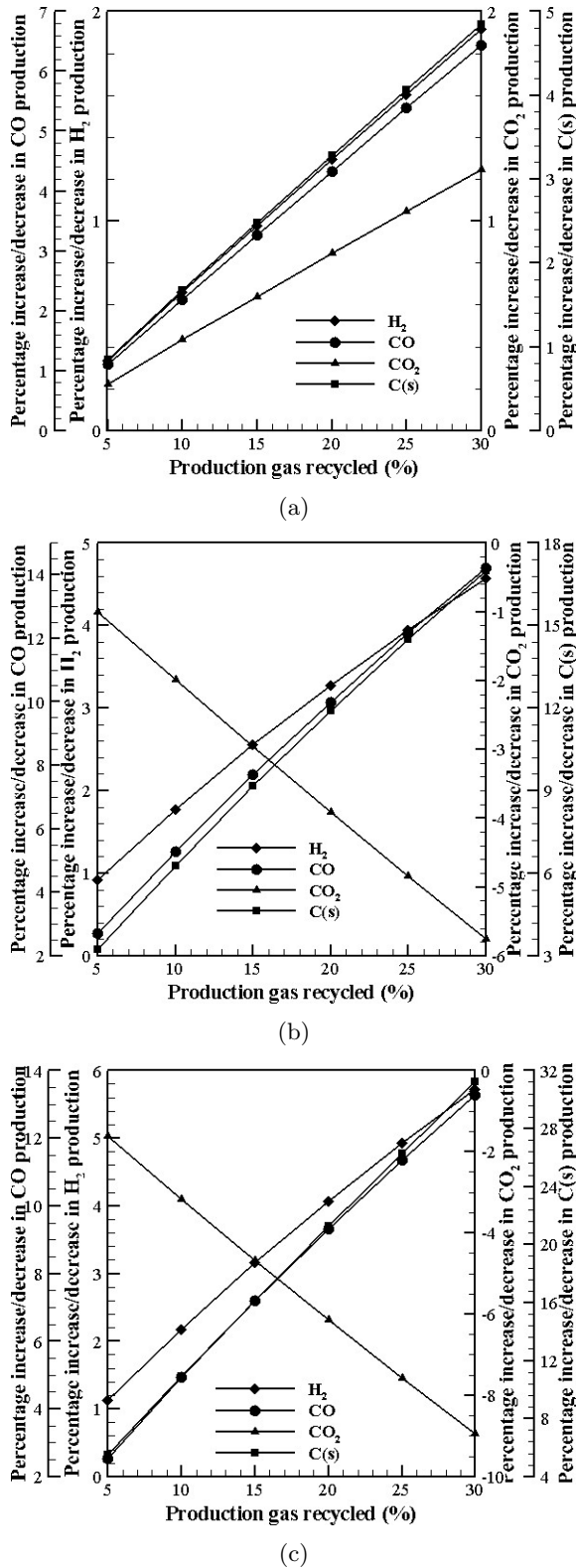
(a)

(b)

(c)

Fig. 6. Evaluation of the effect of gas product recycling on the increase in hydrogen, carbon monoxide, carbon dioxide, and carbon surface coverage at (a) 800 K, (b) 1000 K, and (c) 1200 K, S/C ratio equal to 3, and atmospheric pressure in the presence of rhodium catalyst.

Table 2 summarizes the effects of gas product recycling (GPR) on the steam methane reforming (SMR) process with nickel (Ni) and rhodium (Rh) catalysts at various temperatures (800 K, 1000 K, and 1200 K) and recycling volumes (20% and 30%). The table presents the percentage increase in hydrogen (H_2), carbon monoxide (CO), carbon dioxide (CO_2), and carbon surface coverage (C(s)) for each scenario, along with conclusions on the suitability of GPR under the given conditions.

5 Conclusion

Gas product recycling (GPR) has been proposed as a strategy to improve the performance of the steam methane reforming (SMR) process by reintroducing a portion of the reaction products to the reactor inlet. This study employed a validated and well-suited model based on two reaction chains to investigate the effects of GPR in the presence of nickel and rhodium catalysts. GPR was simulated for volume percentages up to 30% at different temperatures (800, 1000, and 1200 Kelvin), a steam-to-methane ratio of 3, and atmospheric pressure. The key findings of this modeling study are summarized below based on Table 2:

- **Nickel catalyst**
  - 800 K: GPR is not recommended due to undesirable increases in carbon dioxide production and carbon surface coverage.
  - 1000 K: GPR is not recommended due to simultaneous increases in carbon dioxide production and carbon surface coverage.
  - 1200 K: GPR within the range of 20-30% volume is acceptable due to increased syngas production and reduced carbon dioxide leakage.
- **Rhodium catalyst**
  - General Observation: GPR is not recommended for use with a rhodium catalyst at any evaluated temperature due to the significant increase in carbon surface coverage and coke deposition.

These findings suggest that while GPR can be beneficial under specific conditions with nickel catalysts, particularly at higher temperatures, it is generally not suitable for rhodium catalysts due to the adverse effects on catalyst performance and longevity.

Table 2. Summary table

Temperature (K)	Recycling Volume (%)	Catalyst	H_2 Increase (%)	CO Increase (%)	CO_2 Increase (%)	C(s) Coverage Change (%)	Conclusion
800	20	Nickel	2.35	4.44	2.32	-0.29	Not recommended due to increased CO_2 production.
1000	20	Nickel	3.05	7.37	1.44	3.3	Not recommended due to increased CO_2 and C(s) coverage.
1200	20	Nickel	4.24	9.42	-3.32	9.39	Acceptable within 20-30% recycling volume due to increased syngas production and reduced CO_2.
800	30	Rhodium	1.91	6.44	1.24	4.84	Not recommended due to increased CO_2 and C(s) coverage.
1000	30	Rhodium	4.57	14.21	-5.75	17	Not recommended due to increased C(s) coverage.
1200	30	Rhodium	5.73	13.26	-8.95	31.2	Not recommended due to significant increase in C(s) coverage.

Nomenclature

A	Pre-exponential factor in Arrhenius function (variable)
A	Area (m^2)
Θ	Surface coverage parameter (-)
a	Pre-exponential factor in sticking coefficient function (-)
b	Temperature exponent in sticking coefficient function (-)
C	Activation energy in sticking coefficient function (J/mol/K)
E	Activation energy in Arrhenius function (J/mol)
GHSV	Gas hourly space velocity (h^{-1})
k	Chemical species (-)
k	Reaction rate constant (-)
m	Surface coverage parameter (-)
m	Sum of stoichiometric coefficients of surface reactants (-)
n	Amount of substance (mol)
P	Perimeter (m)
P	Pressure (atm)
q	Rate of progress ($mol/m^3/s$)
R	Universal gas constant ($atm\,m^3/mol\,K$)
$\dot{s}$	Net molar production rate in heterogeneous reaction ($kmol/s/m^2$)
T	Temperature (K)
t	Time (s)
u	Velocity (m/s)
W	Molecular weight (kg/mol)

Greek Symbols

Γ	Surface porosity density (mol/m^2)
ρ	Density (kg/m^3)
σ	Number of occupied pores (-)
β	Temperature exponent in Arrhenius function (-)
θ	Mole fraction of occupied pores on the surface (-)
ϵ	Surface coverage parameter (J/mol)
γ	Probability of reaction per collision (-)

Subscripts

s	Solid
i	Chemical reaction
k	Chemical species
f	Forward
in	Inlet
out	Outlet

Chemical Species

H_2O	Water
CH_4	Methane
H_2	Hydrogen
CO	Carbon monoxide
CO_2	Carbon dioxide

References

[1] Bhat SA, Sadhukhan J. Process intensification aspects for steam methane reforming: an overview. AIChE Journal. 2009;55(2):408–422. 170

[2] Nikolaidis P, Poullikkas A. A comparative overview of hydrogen production processes. Renewable and sustainable energy reviews. 2017;67:597–611. 170

[3] Palma V, Ricca A, Meloni E, Martino M, Miccio M, Ciambelli P. Experimental and numerical investigations on structured catalysts for methane steam reforming intensification. Journal of Cleaner Production. 2016;111:217–230. 170

[4] Kuncharam BVR, Dixon AG. Multi-scale two-dimensional packed bed reactor model for industrial steam methane reforming. Fuel Processing Technology. 2020;200:106314. 170

[5] Saeidi S, Fazlollahi F, Najari S, Iranshahi D, Klemeš JJ, Baxter LL. Hydrogen production: Perspectives, separation with special emphasis on kinetics of WGS reaction: A state-of-the-art review. Journal of Industrial and Engineering Chemistry. 2017;49:1–25. 170

[6] Cao C, Zhang N, Chen X, Cheng Y. A comparative study of Rh and Ni coated microchannel reactor for steam methane reforming using CFD with detailed chemistry. Chemical Engineering Science. 2015;137:276–286. 170

[7] Numaguchi T, Kikuchi K. Intrinsic kinetics and design simulation in a complex reaction network; steam-methane reforming. In: Tenth international symposium on chemical reaction engineering. Elsevier; 1988. p. 2295–2301. 170

[8] Xu J, Froment GF. Methane steam reforming, methanation and water-gas shift: I. Intrinsic kinetics. AIChE journal. 1989;35(1):88–96. 170

[9] Wang X, Gorte R. A study of steam reforming of hydrocarbon fuels on Pd/ceria. Applied Catalysis A: General. 2002;224(1-2):209–218. 170

[10] Rakass S, Oudghiri-Hassani H, Rowntree P, Abatzoglou N. Steam reforming of methane over unsupported nickel catalysts. Journal of Power sources. 2006;158(1):485–496. 170

[11] Zhu T, van Grootel PW, Filot IA, Sun SG, van Santen RA, Hensen EJ. Microkinetics of steam methane reforming on platinum and rhodium metal surfaces. Journal of catalysis. 2013;297:227–235. 170

[12] Panagakos G, Kyriakides A, Papadopoulou S, Voutetakis S. A computational investigation of hydrogen production from methane steam reactor. Chemical Engineering Transactions. 2015;45:1033–1038. 170

[13] Arora S, Prasad R. An overview on dry reforming of methane: strategies to reduce carbonaceous deactivation of catalysts. RSC advances. 2016;6(110):108668–108688. 170

[14] German ED, Sheintuch M. Methane steam reforming rates over Pt, Rh and Ni (111) accounting for H tunneling and for metal lattice vibrations. Surface Science. 2017;656:126–139. 170

[15] Abbas SZ, Dupont V, Mahmud T. Kinetics study and modelling of steam methane reforming process over a NiO/Al2O3 catalyst in an adiabatic packed bed reactor. International journal of hydrogen Energy. 2017;42(5):2889–2903. 170

[16] Vasquez Castillo JM, Sato T, Itoh N. Microkinetic analysis of the methane steam reforming on a Ru-supported catalytic wall reactor. Industrial & Engineering Chemistry Research. 2017;56(31):8815–8822. 170, 171

[17] Saeedi A, Allahdadi N. Numerical Investigation of the Performance of Hydrogen Production Process by Production Gas Recirculation. Amirkabir Journal of Mechanical Engineering. 2021;53(1 (Special Issue)):623–638. 170, 172

[18] Saeedi A, Zangooei F. Numerical Investigation of Steam Methane Reforming over Ni-and Rh-based Catalysts to Produce Hydrogen, Syngas and Reduce Surface Coverage. Amirkabir Journal of Mechanical Engineering. 2022;54(7):1587–1606. 170

[19] Goodwin DG, Moffat HK, Weber BW. Cantera: An object-oriented software toolkit for chemical kinetics, thermodynamics, and transport processes; 2021. 171, 172

[20] Kee RJ, Coltrin ME, Glarborg P. Chemically reacting flow: theory and practice. John Wiley & Sons; 2005. 172

[21] Thormann J, Maier L, Pfeifer P, Kunz U, Deutschmann O, Schubert K. Steam reforming of hexadecane over a Rh/CeO2 catalyst in microchannels: Experimental and numerical investigation. international journal of hydrogen energy. 2009;34(12):5108–5120. 172

[22] Ohayre R, Cha SW, Colella W, Prinz FB. Fuel cell fundamentals. John Wiley & Sons; 2016. 172

[23] Maier L, Schädel B, Herrera Delgado K, Tischer S, Deutschmann O. Steam reforming of methane over nickel: development of a multi-step surface reaction mechanism. Topics in catalysis. 2011;54:845–858. 173

[24] Karakaya C, Maier L, Deutschmann O. Surface reaction kinetics of the oxidation and reforming of CH4 over Rh/Al2O3 catalysts. International Journal of Chemical Kinetics. 2016;48(3):144–160. 173

[25] Ryu JH, Lee KY, La H, Kim HJ, Yang JI, Jung H. Ni catalyst wash-coated on metal monolith with enhanced heat-transfer capability for steam reforming. Journal of Power Sources. 2007;171(2):499–505. 173

[26] Schädel BT, Duisberg M, Deutschmann O. Steam reforming of methane, ethane, propane, butane, and natural gas over a rhodium-based catalyst. Catalysis today. 2009;142(1-2):42–51. 173